Received Date : 15-Feb-2016

Revised Date : 07-Jun-2016

Accepted Date : 12-Jun-2016

Article type : B - Brief Communication

Parametric Response Mapping of Bronchiolitis Obliterans Syndrome progression after lung transplantation

Stijn E Verleden[1], Robin Vos[1], Elly Vandermeulen[1], David Ruttens[1], Hannelore Bellon[1], Tobias Heigl[1], Dirk E Van Raemdonck[1] , Geert M Verleden[1], Vibha Lama[2], Brian D Ross[3], Craig J Galbán[3*], and Bart M Vanaudenaerde[1*]

[1] Lung transplant Unit, Department of Clinical and Experimental Medicine, KU Leuven, Leuven Belgium

[2] Pneumology Department, University of Michigan, Ann Arbor, MI, USA

[3] Radiology Department, University of Michigan, Ann Arbor, MI, USA

* Authors contributed equally

Running title: PRM in BOS

Study Correspondence:

Dr. Stijn Verleden

K U Leuven

Lung Transplantation Unit

Herestraat 49, B-3000 Leuven, Belgium

Tel: + 32 16 330194 Fax: + 32 16 330806

E-mail: stijn.verleden@med.kuleuven.be

PRM Correspondence:

Craig J. Galbán, Ph.D.

Associate Professor

University of Michigan

Radiology Department

BSRB, Room A506

109 Zina Pitcher Place

Ann Arbor, MI 48109-2200

Tel: 734-764-8726, Fax: 734-615-1599

Email: cgalban@med.umich.edu

Abbreviations

AT: air trapping

BOS: bronchiolitis obliterans syndrome

CLAD: chronic lung allograft dysfunction

CT: computed tomography

FEV_1: forced expiratory volume in 1 second

FVC: forced vital capacity

HU: Hounsfield unit

LTx: lung transplantation

PD: parenchymal disease

PRM: parametric response mapping

fSAD: Functional small airway disease

rCLAD: restrictive CLAD

Abstract

Bronchiolitis obliterans syndrome (BOS) remains a major complication after lung transplantation. Air trapping and mosaic attenuation are typical radiological features of BOS, however quantitative evaluation remains troublesome.

We evaluated parametric response mapping (PRM, voxel-to-voxel comparison of inspiratory and expiratory CT scans) in lung transplant recipients diagnosed with BOS (n=20) and time-matched stable lung transplant recipients (n=20). Serial PRM measurements were performed pre-diagnosis, at time of BOS diagnosis and post-diagnosis (T_{pre}, T_0 and T_{post} respectively); or at a post-operatively matched time in stable patients. PRM results were correlated with pulmonary function and confirmed by microCT analysis of end-stage explanted lung tissue.

We observed by PRM an increase in functional small airway disease (fSAD), from T_{pre} to T_0 (p=0.006) and a concurrent decrease in healthy parenchyma (p=0.02) in the BOS group. This change in PRM continued to T_{post}, which was significantly different compared to the stable patients (p=0.0002). At BOS diagnosis, the increase in fSAD was strongly associated with a decrease in FEV_1 (p=0.011). MicroCT confirmed the presence of airway obliteration in a sample of a BOS patient identified with 67% fSAD by PRM.

We demonstrated the use of PRM as an adequate readout to monitor BOS progression in lung transplant recipients.

Introduction

Long-term survival after lung transplantation (LTx) is hampered by chronic lung allograft dysfunction (CLAD) which is believed to reflect chronic rejection (1). With one of the highest rejection rates amongst all solid organ transplantations, approximately 50% of LTx recipients suffer from CLAD within five years after transplantation (2). Phenotypes of CLAD with different clinical characteristics and prognoses have been reported in the literature. The most common being bronchiolitis obliterans syndrome (BOS), characterized by an obstructive pulmonary function defect, obliterative bronchiolitis (OB) on histopathologic examination and air trapping and mosaic attenuation on imaging. As a result of the complex pathophysiology of these CLAD phenotypes, treating physicians often face difficulties to obtain an exact and early diagnosis

The gold standard for BOS diagnosis continues to be monitoring of lung function, which is easy to use, cost-effective and provides sufficient repeatability. Lung imaging, primarily via computed tomography (CT), is commonly used to complement spirometry for BOS diagnosis. In BOS, air trapping is visually identified on end-expiration CT scans as parenchymal areas with low attenuation and lack of volume reduction. De Jong and colleagues proposed a composite CT score for BOS diagnosis, comprised of bronchiectasis, mucus plugging, airway wall thickening, consolidation, mosaic pattern and air trapping (AT), which was associated with forced expiratory volume in 1 second (FEV_1) (3). Although this scoring system showed good reproducibility, this is a semi-quantitative technique that requires experienced readers for accurate and repeatable scoring.

Quantitative CT-based analytical measures have shown promise in improving disease diagnosis, phenotypes and prognosis, as well as providing 3D visualization of the disease extent. Parametric response mapping (PRM), a quantitative imaging processing technique applied to inspiration and expiration CT scans was shown to quantify the extent of parenchyma with emphysematous AT and non-emphysematous AT, which is referred to as functional small airways disease (fSAD) in a cohort of COPD patients (4). In a retrospective study of hematopoietic stem cell recipients, PRM was found to be a strong readout of BOS even in the presence of infection (5). Although serial PRM measurements were obtained in only one subject, this technique showed promise in monitoring BOS progression. Here we evaluated PRM as a readout of BOS diagnosis and progression in LTx recipients.

Material and methods

Patient population

Serial paired CT scans were obtained from LTx recipients diagnosed with BOS (n=20) and recipients without CLAD (n=20) as part of a single site retrospective study. Included patients were all double LTx recipients; and both groups were matched for post-operative day of CT, native lung disease, age and gender. All patients have reached a best post-operative FEV_1 >80% predicted and all BOS patients received azithromycin treatment for BOS but were found to be non-responsive. All BOS patients experienced a persistent FEV_1 decrease >20% compared to the mean of the two best post-operative FEV_1 values without a concomitant decrease in TLC≥10% (thus excluding rCLAD) . Inspiratory and expiratory CT scans from BOS recipients were acquired 3 months to 1 year before BOS, T_{pre}, at time of BOS diagnosis, T_0, and at the last available CT, T_{post}, which may have occurred at end of follow-up, last CT prior to a second LTx or death. Time matched CT scans were obtained for the stable

recipients. At the moment of each CT examination, there was no acute rejection, lymphocytic bronchiolitis or infection. This study was approved by the local hospital's ethical committee (S57752).

Computed Tomography

CT data were obtained as whole lung volumetric CT scans at full inspiration (TLC) and incremental scans at relaxed expiration (functional residual capacity) on Siemens Somatom scanner and reconstructed using a b60 or b70 reconstruction kernel. Slice thicknesses were 1.25 mm for all scans, with slice numbers on average around 220 for inspiration scans and 15 for expiration scans. All CT scans were checked for Hounsfield unit (HU) drift and if necessary corrected based on aortic blood (50 HU) and central air (-1000 HU) as previously described (6).

Parametric Response Map

PRM was applied to all paired CT scans from both study groups. Briefly, lungs from both paired CT scans were segmented from the thoracic cavity using an in-house algorithm written in Matlab (The MathWorks, Inc. Natick, MA, USA). The whole-lung CT inspiration scan was spatially registered and aligned to the incremental CT scan obtained at expiration using Elastix, an open source image registration algorithm (7,8). Once complete, the images share the same geometric space where each voxel, the smallest unit of volume in a 3D image dataset, consists of HU values at inspiration and expiration. To minimize the effects of noise on the PRM analysis an adaptive noise-removal filter was applied to both spatially aligned CT scans. Individual voxels were then classified based on predetermined thresholds as normal (green), fSAD (yellow), emphysema (red) and parenchymal disease (purple). Voxels with values ≥-950 HU and <-810 HU at inspiration and ≥-856 HU at expiration were classified normal, ≥ -950 HU and <-810 HU at inspiration and <-856 at expiration were fSAD, <-950 HU at inspiration and <-856 HU at expiration were emphysema and ≥ -810 HU at inspiration were parenchymal disease, PD (5). The emphysema and air trapping thresholds (-950HU and -856HU, respectively) have been previously defined and are used for CT analysis in the COPDGene clinical trial (9–12). The upper limit on the inspiratory CT (-810HU) was determined using healthy smokers accrued as part of the NORM trial (5,13). Global PRM measures were presented as relative lung volumes. The relative volumes for each classification are defined as the sum of all voxels within a class normalized to the sum of all voxels within the volume of the expiratory lungs multiplied by 100. PRM^{Normal}, PRM^{fSAD}, PRM^{Emph} and PRM^{PD} denote the relative volume for each classification.

MicroCT investigation

Further evaluation of the PRM technique was performed by microCT analysis of an explanted lung from a single recipient that had undergone whole-lung inspiration and expiration CT scans

immediately prior to a redo LTx. The lung specimen was collected and scanned using an adapted protocol of our previous work (14,15) (online supplement 1).

Statistical Analysis

All results are shown as median (interquartile range). Differences in continuous variables between BOS and stable patients were determined using a student's T-test. A contingency test was used to assess group difference in discrete data. Paired t-test was used to assess differences between time points (i.e. T_{pre}, T_0 and T_{post}). In addition to the absolute values determined by PRM, the relative change in PRM^{Normal} and PRM^{fSAD} were evaluated between time points and groups. The relative change in PRM metric is defined as $100*[PRM^i(T_j)-PRM^i(T_{pre})]/PRM^i(T_{pre})$, where i is an index to denote normal and fSAD and j denotes time points (T_0, T_{post}). Spearman-rank test was performed for correlation analysis between the relative change in pulmonary function measurements and PRM^{fSAD}. ROC analysis was performed to estimate the specificity and sensitivity of $rPRM^{fSAD}$ at T_0 to detect BOS using the entire study population (n=40). All tests were performed using graph pad prism 6.0 (GraphPad Software, Inc. La Jolla, CA, USA).

Results

Study population

Patient characteristics are presented in table 1. Patients were selected to minimize potentially confounding effects as well as to time-match post-operative CT acquisitions. As such, no significant differences in age, underlying disease, gender and post-operative day of CT scanning between the BOS and stable groups were observed. At T_{pre}, 9 patients from the BOS group had BOS0p versus 5 in the stable group. Four patients in the stable group had BOS0p at T_0 which increased to 9 patients at T_{post}. However none of the stable patients reached BOS1 at any timepoint.

Serial examination of PRM measurements

Representative PRM slices from two cases are shown in Figure 1. Population results for serial PRM^{fSAD} and PRM^{Normal} measurements are shown in Figure 2A and 2B. BOS patients demonstrated a significant increase in PRM^{fSAD} from T_{pre} (18±3%) to T_0 (33±4%; p=0.006). Although the moderate increase in PRM^{fSAD} from T_0 to T_{post} (45±6%) was not significant (p=0.18), PRM^{fSAD} at T_{post} was found to be significant higher compared to T_{pre} values (p<0.0001). In stable patients, a negligible variation in PRM^{fSAD} was observed from T_{pre} to T_0 and T_{post} (p=0.27 and p=0.28 respectively). PRM^{Normal} decreased

from T_{pre} to T_0 (62±4% to 48±4%, p=0.02) in BOS patients with no further decline after diagnosis, T_{post} (38±6%, p=0.36). However, PRM^{Normal} at T_{post} demonstrated a significant decrease from T_{pre} values (p=0.0007). Negligible changes were observed in PRM^{Normal} for the control group (53±4% at T_{pre}, 61±5% at T_0 and 55±6% at T_{post}).

Group Comparisons

Negligible group differences were observed in PRM values of fSAD and healthy parenchyma (p=0.17 and p=0.14, respectively; Figure 2A and B) and FEV_1 (p=0.14; Table 1) at T_{pre}. Interestingly, the mean values for PRM^{fSAD} at T_{pre} were slightly higher in both groups (BOS and stable had 18±3% and 24±4%, respectively) compared to a previously described healthy (non-transplant) control groups (<10% (4) and <15%, supplement material (5)). Although PRM^{fSAD} was higher at T_0 for BOS patients than stable patients, these values were not significant (p=0.09; Figure 2A). The steady increase in PRM^{fSAD} in BOS patients resulted in a significant difference between BOS and stable patients at T_{post} (p=0.0002). Similarly, PRM^{Normal} were significantly lower at T_0 (p=0.02) and T_{post} (p=0.04) in BOS patients when compared to stable patients (Figure 2B). To evaluate if PRM^{fSAD} can detect BOS severity, patients diagnosed with BOS were separated based on BOS grade. Results from this analysis found that patients with BOS 2-3 (n=7) at diagnosis had three times more PRM^{fSAD} (26±7%) than BOS 1 patients (n=13; 9±7%). Although this result was not found to be significant (p=0.10), the general trend suggests PRM^{fSAD} may provide clinical insight into BOS severity. At the end of current follow-up (T_{post}), 11 patients had graft loss (4 death, 7 redo LTx) with 9 patients alive (BOS1, n=4; BOS2, n=4, BOS3, n=1) compared to no graft loss in the stable group. Patients that succumbed to BOS (all BOS 3) had elevated PRM^{fSAD} (59±2%) compared to living patients (25±6%) (p=0.0007), while PRM^{Normal} was significantly lower (21±3% vs. 56±8% respectively, p=0.0007).

Relative Change in PRM

The relative change in PRM^{fSAD} ($rPRM^{fSAD}$) and PRM^{Normal} ($rPRM^{Normal}$) from T_{pre} are presented in Figure 2C-D. As shown in Figure 2C, patients diagnosed with BOS were found to have a relative increase in PRM^{fSAD} of 422±127% at T_0 (p=0.005) and 436±95% at T_{post}. These values were significantly higher than $rPRM^{fSAD}$ observed in stable patients ($rPRM^{fSAD}$ at T_0 of 92±16% (p=0.004) and at T_{post} 116±30% (p=0.001). Presented in Figure 2D, $rPRM^{Normal}$ was found to be lower in BOS patients as compared to stable patients. These values were significantly different between groups at T_0 (p=0.004), but lost significance by T_{post} (p=0.07). The extent of change in $rPRM^{Normal}$ was only significant at T_{post} for BOS patients (p=0.009). By ROC analysis, the relative increase in PRM^{fSAD} at T_0 was found to be significantly associated with BOS (p=0.005). An optimal cutoff of $rPRM^{fSAD}$ at T_0 was found to be 173%, which had 62.5% sensitivity and 93.8% specificity to predict BOS development.

Correlation of PRM^{fSAD} with Spirometric Measures and Air Trapping

Correlations were performed in BOS patients to determine the relationship between PRM and pulmonary function (Figure 3). A relative decline in FEV_1 (%pred) from T_{pre} to T_0 was inversely associated with PRM^{fSAD} (p=0.006 and R=-0.64). Similarly, the decline in FEF25-75 was inversely correlated with PRM^{fSAD} (p=0.031 and R=-0.53). In contrast, no association was observed for the relative change in FVC (%pred) (p=0.43). The inverse correlation between PRM^{fSAD} to both relative changes in FEV_1 (%pred) and FVC (%pred) became stronger from T_{pre} to T_{post} (p=0.0002, R=-0.59 and p=0.0006 and R=-0.53, respectively). A correlation analysis using the absolute value of FEV_1 and FVC in liter yielded similar results (data not shown).

Confirmation by microCT

Presented in Figure 4 are PRM and microCT results from a representative BOS explant specimen. Using CT scans acquired at T_{post}, this patient was found to have PRM measures over both lungs of 15% for healthy parenchyma, 56% for fSAD, 19% for PD and 4% for emphysema. As seen in Figure 4A and B, the PRM, with corresponding scatter plot, at the exact location of the selected core showed a high percentage of fSAD (PRM^{fSAD}=67%) with lower values in PD (PRM^{PD}=16%), normal parenchyma (PRM^{Normal}=9%) and emphysema (PRM_{Emph}=1%). MicroCT confirmed the presence of small airway obliteration on 2 separate locations within the single scanned specimen (Figure 4C and D) which is compatible with obliterative bronchiolitis, the pathological correlate of BOS.

Discussion

In this manuscript, we demonstrated the potential value of serial radiological PRM measurements in diagnosing and monitoring BOS. We provided further support for our findings by demonstrating a correlation between PRM^{fSAD} and FEV_1. Lastly, microCT examination confirmed the presence of small airway obliteration, explaining the fSAD documented with the PRM measurement.

An interesting find in this study was the elevated PRM^{fSAD} observed in all LTx recipients prior to any pulmonary function defect. These values were higher than observed from non-transplant healthy smokers reported in the literature (4,5). Although all patients in this study had a FEV_1>80% predicted at T_{pre}, this find corroborates the observation that air trapping occurs early after LTx, even in stable patients. This is thought to be attributed by some degree of small airway disease secondary

to the transplantation procedure (16). Also, more extended criteria donors, typically older with a longer smoking history, are more commonly used (17).

Recently, Solyanik et al compared 3 methods of quantifying air trapping in LTx patients (18). Their approach differed from the present study in that multiple measurements within the same patients were not obtained. Nevertheless, one method applied a density mapping approach with voxel-to-voxel comparison of inspiratory and expiratory CT analogous to PRM, with the difference being the use of a single threshold applied to the expiratory CT scan. The authors demonstrated a correlation with residual volume/total lung capacity (used to define pathologic air trapping) and the density mapping technique. In parallel, we also quantified air trapping by radiological scoring and compared this to PRM (online supplement 2). Although air trapping progressively increased in BOS patients, we were unable to demonstrate a correlation between FEV_1 decrease and increase in air trapping, demonstrating that PRM might be a more sensitive and objective measurement for estimating small airway obstruction compared to subjective scoring as PRM is probably better in detecting subtle differences in air trapping.

Interestingly, in end-stage BOS lungs 59% of the lung was found to be fSAD by PRM. This find corresponds well with the previously observed percentage of obstructed airways we calculated using our previously reported *ex-vivo* CT analysis of explanted lungs where we found that between 50 and 60% of the airways were obliterated from generation 7 on (14). PRM^{fSAD} generated from the core (67%) slightly differed from what was calculated over the both lungs (56%). This is most likely attributed to spatial heterogeneity of the disease within the lungs. Therefore, severe airway obstruction observed in the analyzed lung strengthens the utility of PRM as a viable tool for monitoring BOS progression.

The objective of this study was to evaluate PRM as an indicator of BOS progression. As such patients with rCLAD were deliberately excluded as they demonstrate elevated attenuation on inspiration CT scans as a result of central and peripheral ground glass opacities (19–21), since PRM has not been validated yet in restrictive lung disease, these patients were not further investigated.

Other possible limitations include the relative low number of patients included in this study, which complicates analyses that require further group stratification. PRM is a quantitative density-based CT technique that applies thresholds for sorting individual voxels into specific classifications. As such various sources of variability may alter the density measurements effecting PRM classifications. In our previous work, we evaluated the effect these sources have on altering the PRM measurements (22). The limitations and generalizability of PRM is further discussed in online supplement 3. However, all CT scans in this study design were quality controlled by assessing HU drift

and corrected when needed. In an effort to reduce the effects of variation in CT acquisitions and reconstruction kernels, a noise-reducing filter was applied to all scans prior to PRM analysis. It is possible that the PRM thresholds used may not fully represent disease state of the studied patient population. PRM^{fSAD} was found to be elevated in pre-BOS recipients relative to healthy smokers, which was consistent to observations from a previous study (5). This may be a consequence of the expiratory threshold (i.e. -856HU) over-estimating the extent of air trapping in the lungs. Confirmation of PRM^{fSAD} by microCT analysis of explanted lungs alleviates some of these possible concerns as OB lesions were observed in regions with high PRM^{fSAD}. The big advantage of our study is the serial measurements from a stable to a diseased state (BOS), which is, to the best of our knowledge, not been performed in this context. It is well understood that spirometric decline is a hallmark of the onset of BOS. Yet clinical practice dictates that CT scans must be used to rule out other pulmonary complications that cause a decline in pulmonary function and to potentially differentiate with rCLAD. As CT scans are part of standard clinical management of these patients, PRM analysis of these scans may complement FEV_1 as an objective readout of the presence and extent of OB as indicated by PRM^{fSAD} and might be specifically useful in patients where spirometry is difficult to interpret such as suture problems, pneumonectomy or single lung transplanted patients (see online supplement 4 for a representative example of a patient with fluctuating FEV_1 but stable PRM^{fSAD} values).

In conclusion, we demonstrate that PRM served as an imaging readout of BOS. Further proof of its applicability is provided by the correlation with spirometry and the presence of OB with microCT. PRM investigation may serve as a complementary tool to aid treating physicians in diagnosing BOS. Further research in this field would include a large, multi-center prospective trial and inclusion of patients with restrictive CLAD. These steps could further confirm the potential use and benefit of PRM for monitoring CLAD progression in LTx recipients.

Acknowledgments

Part of this study was supported by the US National Institutes of Health research grants R01HL122438 and R44HL008837. SEV and RV are sponsored by FWO (12G8715N and 1803516N). RV is supported by the Research Foundation Flanders (FWO) (KAN2014 1.5.139.14) and starting grant UZ Leuven (STG/15/023). GMV and BMV are supported by the FWO (G.0723.10, G.0679.12 and G.0679.12) and KU Leuven research funding C24/15/030.

Disclosure

The authors of this manuscript have conflicts of interest to disclose as described by the American Journal of Transplantation. CJG and BDR have a financial interest in the underlying patented University of Michigan technology licensed to Imbio, LLC., a company in which BDR has a financial interest. The other authors have no conflicts of interest to disclose.

Figure legends

Figure 1

Presented are representative axial slices of PRM from two cases demonstrating the evolution of fSAD in a BOS patient (upper panel) and a stable patient (lower panel) at T_{pre}, T_0 or T_{post} (left to right). The stable case is a male, 40 yrs of age that underwent LTx for COPD. The PRM values at 5 years post-transplantation (T_{pre}) for normal and fSAD were 71% and 12% of the lung volume, respectively. Negligible changes in these PRM values were observed 5.5 yrs (T_0; PRM^{Normal}=77% and PRM^{fSAD}=11%) and 7 yrs (T_{post}; PRM^{Normal}=78% and PRM^{fSAD}=6%) post-transplantation. The BOS case is a 36 year old male transplanted for histocytosis X. PRM^{Normal} and PRM^{fSAD} at 5 years post-transplantation were 76% and 13%, respectively. This patient was diagnosed with BOS 5.5 years post-transplantation (T_0). At T_0, PRM^{Normal} was 30% of the lung volume with PRM^{fSAD} accounting for 56%. Prior to redo-transplantation (6 years post-transplantation), PRM^{fSAD} changed slightly from the T_0 value (58%), yet PRM^{Normal} decreased to 18% of the lung volume. The resulting loss of PRM^{Normal} is attributed to an increase of low attenuation regions identified by PRM as emphysema (1% at T_0 to 12% at T_{post}). BOS, bronchiolitis obliterans syndrome; COPD, chronic obstructive pulmonary disease; fSAD, functional small airway disease; LTx, lung transplantation; PRM, parametric response mapping.

Figure 2

Group comparisons of serial measurements of PRM. Line plots are used to present the group differences observed for the absolute and relative change in (A and C) PRM^{fSAD} and (B and D) PRM^{Normal} obtained at T_{pre}, T_0 and $T_{post.}$ Significant differences between timepoints for the BOS groups is denoted as * for $p<0.05$, ** for $p<0.01$, *** for $p<0.001$. Significant differences between

groups is denoted as # for p<0.05, ## for p<0.01, ### for p<0.001. Data is presented as the mean ± standard error of the mean. PRM, parametric response mapping.

Figure 3

Assessment of the relationship between PRM and pulmonary function. Correlation analyses are presented for the relative change in PRM^{fSAD} to the relative change in FEV_1 from (A) T_{pre} to T_0 and (B) T_{pre} to T_{post}. PRM, parametric response mapping.

Figure 4

Confirmation of OB by microCT in a lung region of high PRM^{fSAD}. (A) Presented are serial *in vivo* expiration CT scans with PRM image or cored region from superior to inferior and the explant slice with the location of the scanned core indicated by a blue dashed circle. (B) Corresponding PRM scatter plot for the cored region. The PRM at the exact location of the selected core showed a high percentage of fSAD, yellow (PRM^{fSAD}=67%); while high attenuation regions, purple (PRM^{PD}=16%) and normal parenchyma, green (PRM^{Norm}=9%) were less frequent, while emphysema was almost absent, red (PRM_{Emph}=1%). (C) MicroCT images of the core showing initially a patent airway (yellow arrow), which completely obliterates (red arrow). (D) MicroCT images within the same core at a different location illustrating another airway lesion where a patent airway (yellow arrow) is found to completely obliterate (red arrow). PRM, parametric response mapping.

Supporting Information

Additional Supporting Information may be found in the online version of this article.

Supplemental Materials and Methods

Figure S1: (A) deformable registration of the in vivo inspiration, in vivo expiration and explant lung CT. (B) Linear registration of the explant CT with the specific (drilled) lung section. (C) Final transformation of the in vivo and expiration CT.

Figure S2: Comparison of PRM_{fSAD} to CT scored airtrapping

Figure S3: Pulmonary function evolution of a 36 year old female patient transplanted for non-specific interstitial fibrosis with additional endobronchial stenting within 2 months after transplantation for collapse of the right bronchus. The FEV_1 fluctuates during her later follow-up declining below the BOS threshold (≥20 FEV_1 decline; red line) on several separate occasions. Despite this fluctuating pulmonary function, the patients remains BOS-free at the end of follow-up. Two pulmonary function decreases could be explained by overt infection which are indicated in the graph. The PRM measurements of the acquired CT's during her follow-up show a relatively stable percentage of PRM^{fSAD} and PRM^{Normal}.

REFERENCES

1. Verleden GM, Raghu G, Meyer KC, Glanville AR, Corris P. A new classification system for chronic lung allograft dysfunction. J Heart Lung Transplant. 2014 Feb;33(2):127–33.

2. Yusen RD, Edwards LB, Kucheryavaya AY, Benden C, Dipchand AI, Goldfarb SB, et al. The Registry of the International Society for Heart and Lung Transplantation: Thirty-second Official Adult Lung and Heart-Lung Transplantation Report-2015; Focus Theme: Early Graft Failure. J Heart Lung Transplant. 2015 Oct;34(10):1264–77.

3. De Jong PA, Dodd JD, Coxson HO, Storness-Bliss C, Paré PD, Mayo JR, et al. Bronchiolitis obliterans following lung transplantation: early detection using computed tomographic scanning. Thorax. 2006 Sep;61(9):799–804.

4. Galbán CJ, Han MK, Boes JL, Chughtai KA, Meyer CR, Johnson TD, et al. Computed tomography-based biomarker provides unique signature for diagnosis of COPD phenotypes and disease progression. Nat Med. 2012 Nov;18(11):1711–5.

5. Galbán CJ, Boes JL, Bule M, Kitko CL, Couriel DR, Johnson TD, et al. Parametric response mapping as an indicator of bronchiolitis obliterans syndrome after hematopoietic stem cell transplantation. Biol Blood Marrow Transplant. 2014 Oct;20(10):1592–8.

6. Stoel BC, Stolk J. Optimization and standardization of lung densitometry in the assessment of pulmonary emphysema. Invest Radiol. 2004 Nov;39(11):681–8.

7. Klein S, Staring M, Murphy K, Viergever MA, Pluim JPW. elastix: a toolbox for intensity-based medical image registration. IEEE Trans Med Imaging. 2010 Jan;29(1):196–205.

8. Shamonin DP, Bron EE, Lelieveldt BPF, Smits M, Klein S, Staring M, et al. Fast parallel image registration on CPU and GPU for diagnostic classification of Alzheimer's disease. Front Neuroinform. 2013;7:50.

9. Regan EA, Hokanson JE, Murphy JR, Make B, Lynch DA, Beaty TH, et al. Genetic epidemiology of COPD (COPDGene) study design. COPD. 2010 Feb;7(1):32–43.

10. Gevenois PA, de Maertelaer V, De Vuyst P, Zanen J, Yernault JC. Comparison of computed density and macroscopic morphometry in pulmonary emphysema. Am J Respir Crit Care Med. 1995 Aug;152(2):653–7.

11. Gevenois PA, De Vuyst P, de Maertelaer V, Zanen J, Jacobovitz D, Cosio MG, et al. Comparison of computed density and microscopic morphometry in pulmonary emphysema. Am J Respir Crit Care Med. 1996 Jul;154(1):187–92.

12. Newman KB, Lynch DA, Newman LS, Ellegood D, Newell JD. Quantitative computed tomography detects air trapping due to asthma. Chest. 1994 Jul;106(1):105–9.

13. Boudewijn IM, Postma DS, Telenga ED, Ten Hacken NHT, Timens W, Oudkerk M, et al. Effects of ageing and smoking on pulmonary computed tomography scans using parametric response mapping. Eur Respir J. 2015 Oct;46(4):1193–6.

14. Verleden SE, Vasilescu DM, Willems S, Ruttens D, Vos R, Vandermeulen E, et al. The site and nature of airway obstruction after lung transplantation. Am J Respir Crit Care Med. 2014 Feb 1;189(3):292–300.

15. Verleden SE, Vasilescu DM, McDonough JE, Ruttens D, Vos R, Vandermeulen E, et al. Linking clinical phenotypes of chronic lung allograft dysfunction to changes in lung structure. Eur Respir J. 2015 Nov;46(5):1430-9.

16. Bankier AA, Van Muylem A, Knoop C, Estenne M, Gevenois PA. Bronchiolitis obliterans syndrome in heart-lung transplant recipients: diagnosis with expiratory CT. Radiology. 2001 Feb;218(2):533–9.

17. Somers J, Ruttens D, Verleden SE, Cox B, Stanzi A, Vandermeulen E, et al. A decade of extended-criteria lung donors in a single center: was it justified? Transpl Int. 2015 Feb;28(2):170–9.

18. Solyanik O, Hollmann P, Dettmer S, Kaireit T, Schaefer-Prokop C, Wacker F, et al. Quantification of Pathologic Air Trapping in Lung Transplant Patients Using CT Density Mapping: Comparison with Other CT Air Trapping Measures. PLoS ONE. 2015;10(10):e0139102.

19. Verleden SE, de Jong PA, Ruttens D, Vandermeulen E, van Raemdonck DE, Verschakelen J, et al. Functional and computed tomographic evolution and survival of restrictive allograft syndrome after lung transplantation. J Heart Lung Transplant. 2014 Mar;33(3):270–7.

	BOS	Stable	p-value
Number of patients, n	20	20	
Donor smoking, n (%)			0.56
yes	3 (15%)	5 (25%)	
no	13 (65%)	13 (65%)	

20. Sato M, Waddell TK, Wagnetz U, Roberts HC, Hwang DM, Haroon A, et al. Restrictive allograft syndrome (RAS): a novel form of chronic lung allograft dysfunction. J Heart Lung Transplant. 2011 Jul;30(7):735–42.

21. Todd JL, Jain R, Pavlisko EN, Finlen Copeland CA, Reynolds JM, Snyder LD, et al. Impact of forced vital capacity loss on survival after the onset of chronic lung allograft dysfunction. Am J Respir Crit Care Med. 2014 Jan 15;189(2):159–66.

22. Boes JL, Bule M, Hoff BA, Chamberlain R, Lynch DA, Stojanovska J, et al. The Impact of Sources of Variability on Parametric Response Mapping of Lung CT Scans. Tomography. 2015 Sep;1(1):69–77.

unknown	4 (20%)	2 (10%)	
Donor age, yr	42±4	43±3	0.93
Recipient age, yr	46±3	49±3	0.54
Recepient gender, n(%)			0.75
Male	8 (40%)	9 (45%)	
Female	12 (60%)	11 (55%)	
Underlying disease, n(%)			0.75
COPD	9 (45%)	11 (55%)	
CF+BRECT	3 (15%)	5 (25%)	
ILD	2 (10%)	1 (5%)	
Redo	4 (20%)	2 (10%)	
Eisenmenger	1 (5%)	1 (5%)	
Histiocytosis X	1 (5%)	0	
POD of CT, yr			
Timepoint 1, T_{pre}	2.7±0.4	2.6±0.4	0.90
Timepoint 2, T_0	3.3±0.5	3.5±0.5	0.80
Timepoint 3, T_{post}	4.9±0.4	5.0±0.6	0.82
FEV_1 at CT, L			
Timepoint 1, T_{pre}	2.65±0.16	3.01±0.17	0.14
Timepoint 2, T_0	1.88±0.15	3.12±0.17	<0.0001
Timepoint 3, T_{post}	1.11±0.15	3.02±0.19	<0.0001
FEF25-75 at CT, L			
Timepoint 1, T_{pre}	2.54±0.26	3.05±0.29	0.19
Timepoint 2, T_0	1.17±0.24	2.97±0.29	<0.0001
Timepoint 3, T_{post}	0.41±0.07	2.79±0.24	<0.0001
BOS stage at diagnosis, n (%)			
BOS1	13 (65%)	NA	
BOS2	4 (20%)	NA	
BOS3	3 (15%)	NA	

Table 1: patient characteristics of the 20 BOS and 20 stable patients included in the PRM study.

Abbreviations: COPD: chronic obstructive pulmonary disease, CF: cystic fibrosis; BRECT: bronchiectasis, ILD: interstitial lung disease, Redo: redo lung transplantation; POD: post-operative day; CT: computed tomography; BOS: bronchiolitis obliterans syndrome. Contingency tables were used to compare group differences, unpaired T-test was used for continuous data.

Figure 1

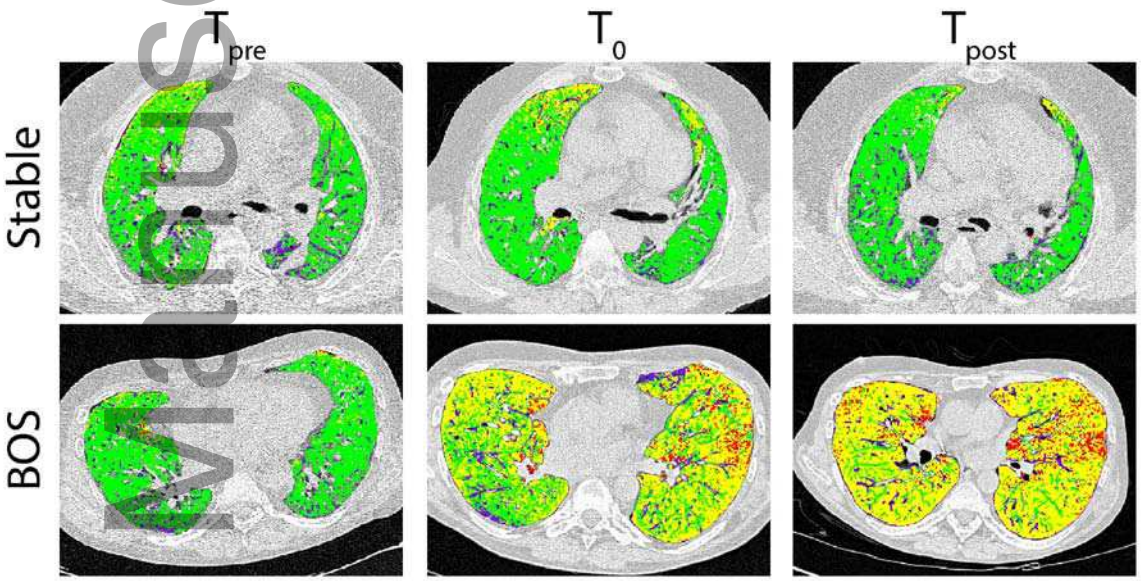

Figure 2

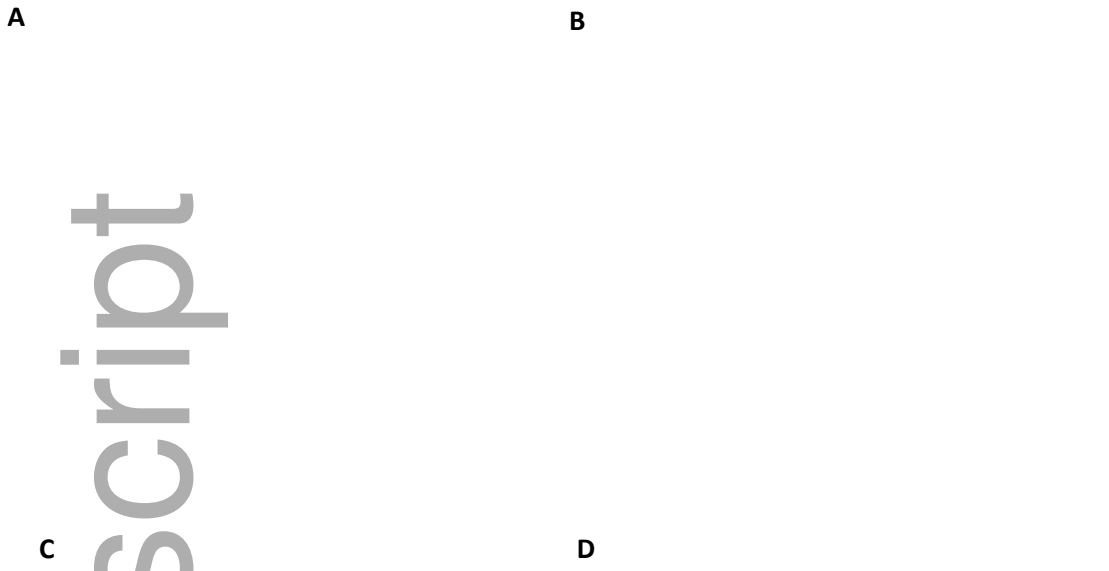

Figure 3

Figure 4